Desalination 476 (2020) 114229

Contents lists available at ScienceDirect

Desalination

journal homepage: www.elsevier.com/locate/desal

Impacts of flow channel geometry, hydrodynamic and membrane properties on osmotic backwash of RO membranes—CFD modeling and simulation

Kwanho Jeong[a,b], Minkyu Park[c], Seungjae Oh[d], Joon Ha Kim[a,*]

[a] School of Environmental Science and Engineering, Gwangju Institute of Science and Technology (GIST), Gwangju 500-712, Republic of Korea
[b] Singapore Membrane Technology Centre, Nanyang Environment and Water Research Institute, Nanyang Technological University, Singapore 637141, Singapore
[c] Department of Chemical and Environmental Engineering, University of Arizona, Tucson, AZ 85721, USA
[d] School of Mechatronics, Gwangju Institute of Science and Technology (GIST), Gwangju 500-712, Republic of Korea

ARTICLE INFO

Keywords:
Reverse osmosis
Membrane cleaning
Osmotic backwash
Computational fluid dynamics
Spacers

ABSTRACT

The presence of the spacer and biofilm can accompany the high complexity of the mass and momentum transport in an osmotic backwash (OBW) process of reverse osmosis (RO) membranes. For more reliable simulations, it would be essential to consider such highly complex transport phenomena across the membranes and through membrane flow channels. Therefore, we simulated the effects of spacer designs, hydrodynamic, and membrane properties on OBW in the scenario of biofouling on RO membrane surfaces. To this end, the OBW process was numerically modeled in two-dimensional spacer-filled crossflow channels based on the finite element method. Subsequently, the concentration and velocity fields inside of the membrane, biofilm, and flow channels were analyzed. Results showed that the submerged spacer could enhance the water and salt mass transfer in the membrane channel, to a greater extent than the cavity and zigzag spacers, which can ultimately enhance the OBW efficiency for a foulant removal. Additionally, the OBW performance is chiefly impacted by the structure parameter of the porous support layer. Also, the existence of biofilm in the feed channel can render the feed concentration and membrane water permeability more sensitive to the OBW process than the non-fouled channel.

1. Introduction

Reverse osmosis (RO) is one of the most widely applied water treatment processes in various treatment applications such as drinking water and wastewater treatments, water reuse, desalination, and other purification processes [1]. This is attributed to the comparative ease of system design and operation, the high removal efficiency of contaminants in aqueous solutions, and no harmful byproduct formation [1,2]. Despite the benefits of RO membrane processes, however, membrane fouling is the primary hindrance to its cost-efficient operations [1,3]. Notably, a highly compacted irreversible fouling layer that firmly adheres to membrane surfaces cannot be readily removed even under harsh chemical and physical cleaning methods [4]. Therefore, advanced cleaning methods to recover membrane performance from a severe membrane fouling would be essential for an efficient and sustainable RO membrane operation to reduce capital and operation/maintenance (O&M) costs [5–7].

Various cleaning methods can mitigate the irreversible fouling to maintain a longer membrane lifespan with a more sustainable performance during RO filtration. The frequent and periodic implementation of osmotic backwash (OBW) could be one of the promising techniques to effectively alleviate the formation of a severe fouling layer without chemical cleaning reagents [6]. A highly dense and compact fouling layer on the RO membrane surface can turn into being swelling, lifting, and sweeping during OBW operation [6]. In addition, a synergistic effect of OBW and chemical cleaning on foulant removal has also been reported. Chemical agents loosened the attachment of the fouling layer with the membrane surface, and subsequently, simultaneous applications of the crossflow-induced shear and the permeation drag due to OBW could effectively flush the loosened fouling layer [5]. Fundamentally, the OBW process is driven spontaneously by the chemical potential gradient (equivalently, osmotic pressure difference) between permeate and feed solutions in fluid channels across the membrane. This osmotic backflow of water from the permeate to feed sides can also be induced if the hydraulic transmembrane pressure (TMP) is below the transmembrane osmotic pressure [8]. The osmotic backflow is generally accomplished by either reducing the feed-side applied pressure below the osmotic pressure difference given solutions,

* Corresponding author.
E-mail address: joonkim@gist.ac.kr (J.H. Kim).

https://doi.org/10.1016/j.desal.2019.114229
Received 9 July 2019; Received in revised form 23 October 2019; Accepted 17 November 2019
Available online 24 November 2019
0011-9164/ © 2019 Elsevier B.V. All rights reserved.

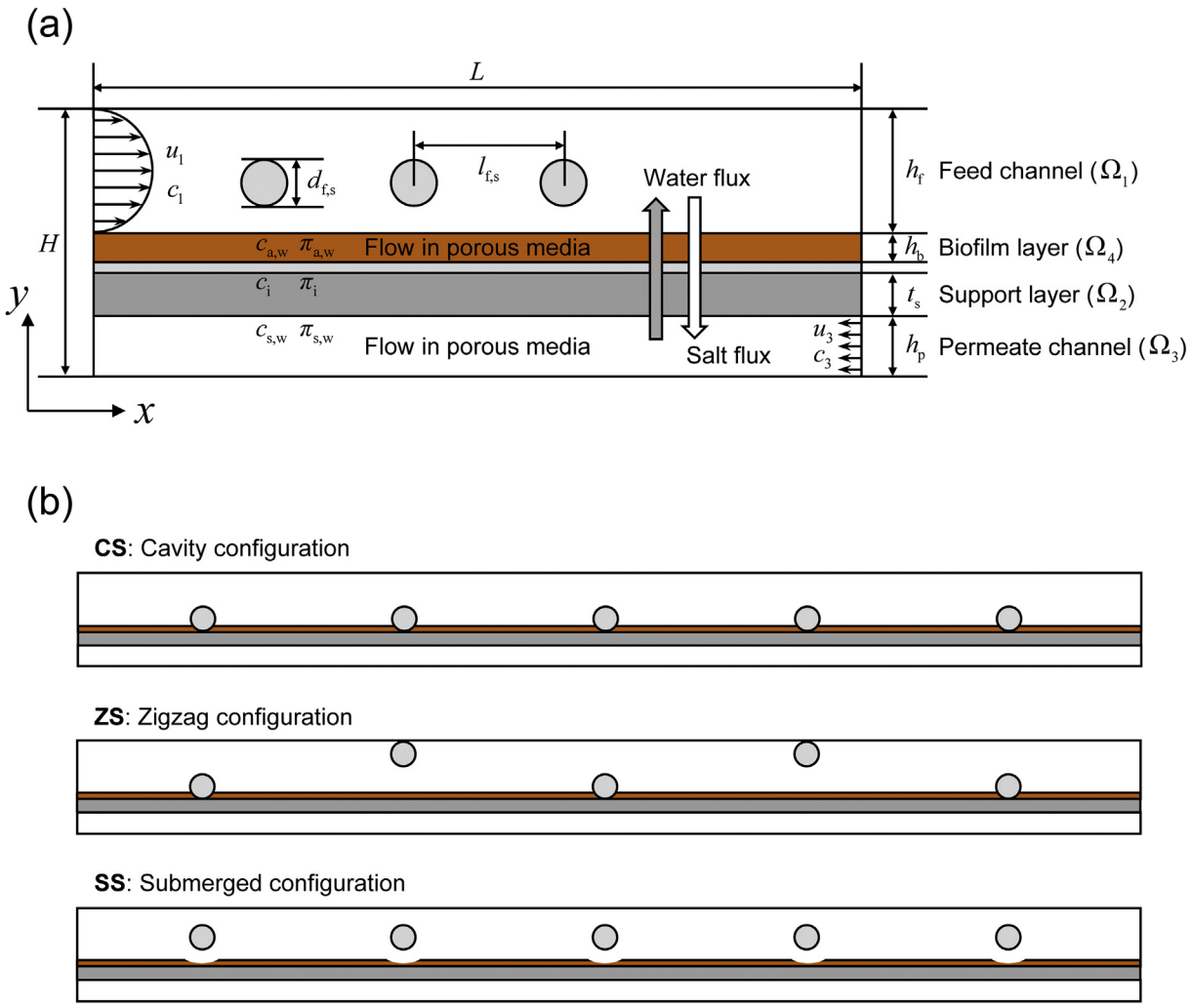

Fig. 1. Illustration of (a) simulation domains of osmotic backwash (OBW) process and (b) transverse filament configurations of spacers used as flow channel geometry.

raising the permeate-side pressure, or injecting a pulse of a hypersaline solution (17–25% NaCl) into the feedwater over a few seconds. The latter two ways, however, are at risk of damaging the composite membranes and elements, because of the high backpressure and the excessive cleaning force over 100 bar, respectively [9,10].

To date, there have been a few reported studies exploring transport behavior in the OBW process of RO membranes. These provided insight into effective OBW methods. Qin et al. [11], Ramon et al. [5], Bar-Zeev and Elimelech [12], and Park et al. [13] conducted experiments with fouled membranes under normal operating conditions, to evaluate cleaning efficiency of OBW with practical implications. They confirmed the enormous potential of foulant removal and flux restoration with the employment of the OBW process in RO membranes. To be specific, OBW (with a 1.6 M NaCl solution) for the alginate-fouled RO membrane achieved > 90% permeate flux recovery from the initial flux [5], while that (with a 1.5 M NaCl solution) for the biofouled RO membrane resulted in 63% permeate flux recovery with a significant reduction in the biovolume (70–79%) along with substantial removal of total organic carbon and proteins (78 and 66%, respectively) [12]. On the other hand, Sagiv et al. [14–16] and Ramon et al. [9] focused more on the space- and time-dependent changes in flow and mass transfer inside the feed and permeate channels during osmotic backwashing. To this end, they performed numerical modeling and simulations on the transient behavior of the backwashed flux and its accumulated volume with respect to time as well as salt concentrations of membrane surface and bulk flow channels, under different operating conditions (backwash time, flow velocity, pressure, and concentration).

The previous modeling studies have addressed the dynamic behavior of OBW processes in an open fluid channel [9,15]. Although such a modeling approach can shed light on the understanding of the OBW, the open channel condition in the absence of membrane fouling may oversimplify fluid dynamics and mass transfer. In practice, spacers maintain space between membranes in a spiral-wound module (SWM) and promote turbulence in the crossflow channels. The disregard of the high complexity of mass and momentum transport in an SWM, promoted by the presence of spacers, may incur discrepancies between simulations in the spacer-filled channel, which can be further significant if membrane fouling is not considered in the modeling. The spacers, in particular, have a considerable impact on spatial changes in pressure, velocity, and concentration in the flow channel [17–20]. For instance, feed spacers in the RO process allow enhancement in mass transport in a boundary layer since flow unsteadiness and turbulence are promoted [19]. OBW flux along the flow channel also may be primarily influenced by local fluid conditions such as crossflow velocity and salt concentration in a similar vein. This is because such net-type turbulence promoters can affect the concentration difference between the feed and permeate sides in the vicinity of the membrane active layer. Therefore, considering their effects on the OBW process would be crucial for more reliable and realistic computational fluid dynamics (CFD) simulation results.

Table 1
Simulation conditions for osmotic backwash (OBW) model.

Parameter (unit)	Symbol	Value	Unit
Geometrical parameters			
Channel length	L	0.015	m
Channel height	h_f	7.0×10^{-4}	m
	h_p	2.5×10^{-4}	m
Feed spacer diameter	$d_{f,s}$	3.6×10^{-4}	m
Distance between transverse filaments	$l_{f,s}$	2.5×10^{-3}	m
The number of feed spacers		5	ea
Physical parameters			
Osmotic pressure[a]	π	$4.5032 \times c^2 + 43.6426 \times c$	bar
Diffusion coefficient of NaCl	D	1.5×10^{-9}	$m^2\ s^{-1}$
Permeate-side hydraulic permeability	κ_p	2.0×10^{-10}	m^2
Permeate-side porosity	ε_p	0.5	
Membrane properties			
Water permeability	A	1.35–1.90	$L\ m^{-2}\ h^{-1}\ bar^{-1}$
Solute permeability	B	0.02–0.03	$L\ m^{-2}\ h^{-1}$
Membrane structure parameter	S	685–1370	μm
Biofilm properties			
Layer thickness	h_b	1.0×10^{-4}	m
Hydraulic permeability	κ_b	10^{-16}	m^2
Porosity[b]	ε_b	0.8	
Operating conditions			
Average inlet velocity of channels[c]	$u_{1,inlet}$	0.1–20	cm/s
	$u_{3,inlet}$	0.1	cm/s
Inlet concentration of NaCl	$c_{1,inlet}$	0.6–1.2	$mol\ L^{-1}$
	$c_{3,inlet}$	0.01–0.02	$mol\ L^{-1}$
Transmembrane pressure	Δp	0–20	bar

[a] The unit of c in the equation is M ($=$mol L^{-1}).
[b] The unit of ε_b is defined as m^3 liquid per m^3 biomass.
[c] The permeate channel inherently possesses the cross-flow velocity much lower than the feed channel in typical operation of commercially available spiral wound RO membrane modules. The permeate spacer is a densely knitted fabric made of woven thin plastic fibers [21].

The primary aim of this study is to evaluate the OBW process in RO membrane processes with various conditions of simplified spacer designs and process variables. To this end, OBW in two-dimensional (2D) spacer-filled channels were simulated using the finite element method (FEM). With this model, we analyzed the concentration and velocity fields inside of membrane and flow channels, in order to investigate the effect of channel geometry on the mass transfer of water and salt. Subsequently, the extent of concentration polarization (CP) was predicted, and its relative contribution to water flux degraded by CP effect was estimated. We also assessed OBW flux under different operating conditions of the inlet concentration and velocity, and TMP. The sensitivity analysis was finally performed to assess the important design and operational parameters in OBW processes.

2. Modeling procedures

2.1. Simulation domains and conditions

The simulation domain consists of four regions: Ω_1, Ω_2, Ω_3, and Ω_4 (Fig. 1a). Domain 1, Ω_1, represents a spacer-filled membrane channel for the feed solution, while Domain 2, Ω_2, is a porous support layer of the membrane. Domains 3 and 4, Ω_3, and Ω_4, are the permeate channel in which spacer is a densely knitted fabric [21] and a biofilm layer formed by membrane fouling, respectively. In this modeling, both domains are considered as flow in porous media, so that the governing equations in Ω_3 and Ω_4 were identical to each other but distinct from those for the flow in Ω_1. The domain Ω_2, one the other hand, can be modeled differently from Ω_3 and Ω_4 without the flow model, despite the porous structure of the support layer. Note that Section 2.2 deals with the governing equations and boundary conditions for the domains in detail. It is noted in the figure that the subscripts (a,w, i, and s,w) of the concentration and osmotic pressure symbols (c and π) denote the active layer wall (active layer surface), active layer–support layer interface, and support layer wall (support layer surface), respectively.

It is noteworthy to point out that the transport phenomena of the OBW process are similar to those of pressure retarded osmosis (PRO) process, an osmotically driven membrane process that is mainly used to produce energy from the salinity gradient. Both membrane processes resemble each other in that 1) water transports towards higher concentration from lower concentration, and 2) the membrane activated layer faces to the solution with higher concentration. The feed and permeate solutions flow into given channels in a counter-current manner. Note that we modeled the domains and equations of the OBW process with similar characteristics of mass and momentum transfer and geometry in the PRO process. Both processes in the SWM resemble each other because of physical features as follows: mass transfer directions of water and solute components; a membrane orientation in which the active and support layers are in contact with the higher and lower saline solutions, respectively. As a result, the dilutive and concentrative external concentration polarization (ECP) occurs on both sides of membrane surfaces facing the high and low concentration channels, respectively, while internal concentration polarization (ICP) develops inside the support layer.

In a commercially available SWM, channel spacers play significant roles in convective flow and mass transfer in boundary layers [18], therefore affecting the OBW process. Three different configurations of transverse cylindrical filaments were taken into account: cavity, submerged, and zigzag patterns of spacer configurations with the same size and shape (Fig. 1b). Hereafter, these spacers are named in abbreviated forms of CS, SS, and ZS, respectively. Such spacer designs have been widely used for CFD simulations of 2D flow channels in SWMs [20]. Five transverse filaments are embedded and spacing of 2.5 mm ($l_{f,s}$) in the feed channel with 15 mm of length (L). The feed and permeate channel heights, h_f and h_p respectively, are 0.7 mm and 0.25 mm [21], while the thicknesses for the support and biofilm layers, t_s and h_b, are 150 μm and 100 μm [22], respectively. The model simplifies a biofilm

Table 2
Boundary conditions.

	Momentum	Mass
Inlet[a]	$u_1(x = 0) = 6\,\overline{u_0}\,y(h - y)/h^2$ $u_3(x = L) = u_0$	$c_1(x = 0) = c_{f,b}$ $c_3(x = L) = c_{p,b}$
Hard wall	$\mathbf{u} = 0$	$\mathbf{n} \cdot (-D \nabla c + c\mathbf{u}) = 0$
Active layer[b]	$v_w = A(\Delta\pi - \Delta p)$	$\mathbf{n} \cdot (-D \nabla c) + v_w c_{a,w} = B\Delta c$
Support layer[c]	$v = v_w$	$\mathbf{n} \cdot (-D \nabla c_3 + c_3\mathbf{u}_3) = \mathbf{n} \cdot (-D_e \nabla c_2 + c_2\mathbf{u}_2)$
Open	$\mu[\nabla\mathbf{u} + (\nabla\mathbf{u})^t] \cdot \mathbf{n} = 0, p = 0$	$\mathbf{n} \cdot (-D \nabla c) = 0$

[a] The subscripts of the bulk feed and permeate solutions are indicated, respectively, by f,b and p,b, while u_0 denotes the velocity at the inlet.
[b] $\Delta\pi$ and Δc are the differences in osmotic pressure and concentration between each side of the active layer, defined as $\pi_{a,w}(c_{a,w}) - \pi_i(c_i)$ and $c_{a,w} - c_i$, respectively. The subscripts, a,w and i, denote the active layer surface and active layer–support layer interface, respectively.
[c] $D_e = D\varepsilon/\tau$, where D is the diffusion coefficient of the solute, ε is the porosity, and τ is the tortuosity.

layer with the assumption that biofilms cover the membrane homogeneously, expect for SS at spacer regions to reflect its inherent characteristics of flow pattern and biofilm formation [22].

Table 1 summarizes the values of input parameters used in the modeling. NaCl solution was considered as feed and permeate solutions. We attained the physicochemical properties of the solutions from the literature [17]. The osmotic pressure was computed using a second-order polynomial equation, which fitted to data at a PH of 7 and a temperature of 25 °C with OLI stream analyzer (OLI Systems Inc., Morris Plains, NJ) [17]. The dimensions of simulated channel geometries, including transverse spacer filaments, were determined based on those applied in commercially available spiral-wound reverse osmosis modules [23]. The permeate channel and biofilm properties were sourced from [21,22].

2.2. Governing equations and boundary conditions

The normal RO operation and OBW are dynamically alternating in practice, but it is challenging for CFD modeling and simulation of the OBW process to consider the dynamic state of simultaneous mass transport of water, salt, and foulant over time. Therefore, in this study, we simplified the OBW process of the RO membrane by assuming that the backwash efficiency is primarily dependent on the initial backwash flux. This assumption allows for the application of a steady-state simulation. The momentum and mass transport are determined using Eqs. (1)–(4), in order to obtain the velocity and concentration profiles of Domains 1–4 (Ω_1–Ω_4 in Fig. 1a). The fluid is assumed to be Newtonian, incompressible, and laminar in a steady state. Flow in the spacer-filled domain (Ω_1 in Fig. 1a) is described by the Navier-Stokes equations of motion. Flows in the domains for permeate solution channel and biofilm (Ω_3 and Ω_4 in Fig. 1a, respectively), on the other hand, is described by the Brinkman equations to account for momentum transport through viscous effects and pressure gradients in porous media [24]. It is assumed that the flow in Ω_4 occurs in a longitudinal direction. For the support layer domain (Ω_2 in Fig. 1a) where ICP is computed, we assume that [17]: 1) porous structure is homogeneous, hence the effective diffusivity of such layer, D_e ($=D\varepsilon/\tau$), is constant irrespective of location; 2) axial velocity, u, is inexistent in the support layer and thus vertical velocity, v, varies only in the horizontal direction. The second assumption particularly facilitate applying a mass balance solution to Ω_2 [25]: the boundary conditions of the momentum equation at the support layer surface (i.e., the interface between the support layer and permeate solution) is enabled to be equal to the active layer surface (i.e., the interface between the active layer and feed solution) at the same axial positions; hence, the vertical velocities at the corresponding axial positions in Ω_2 are identical to those of the support layer interface.

Continuity:

$$\nabla\cdot\mathbf{u} = 0 \tag{1}$$

Navier-Stokes:

$$\nabla\cdot\boldsymbol{\sigma} = \rho(\mathbf{u}\cdot\nabla)\mathbf{u}$$
$$\boldsymbol{\sigma} = \mathbf{T} - P\mathbf{I};\ \mathbf{T} = \mu[\nabla\mathbf{u} + (\nabla\mathbf{u})^t] \tag{2}$$

Brinkman [22]:

$$\frac{\eta}{\kappa}\mathbf{u} + \nabla p = \frac{1}{\varepsilon}\left[\eta\cdot\nabla^2\mathbf{u} - \left(\frac{2\eta}{3} - \kappa\right)(\nabla\cdot\mathbf{u})\right] \tag{3}$$

Convection-Diffusion:

$$\mathbf{u}\cdot\nabla c = \nabla\cdot(D\nabla c) \tag{4}$$

where $\mathbf{u}$ is the vector of velocity that consists of u and v in the 2D domain. ∇ is the vector differential operator for gradient and divergence. $\boldsymbol{\sigma}$ is the total stress tensor—which is a function of the viscosity stress and identity tensors, and the pressure (i.e., $\mathbf{T}$, $\mathbf{I}$, and P, respectively). μ and η denote the dynamic viscosity of the fluid, κ is the hydraulic permeability, ε is the porosity, c is the solute concentration, and D is the diffusion coefficient.

Boundary conditions are applied to the inlet and outlet of solution channels, impermeable wall, active and support layers of the membrane (Table 2). The parabolic velocity profile is used for the feed solution channel as the inlet boundary conditions of the momentum equation, while it is improper to impose such a fully developed velocity profile on the permeate solution channel assimilated into porous media. Open boundary conditions are used as the boundary conditions at both channels' outlets. No-slip and no penetration occur on the boundaries of impermeable walls. In this study, the water and salt transport across the membrane is described by a solution-diffusion model. Next, a Neumann boundary condition is employed to compute the solute mass balance at the interface between the active layer and solution channel interface [17,26].

2.3. Sensitivity analysis

Latin Hypercube One-factor-At-a-Time (LH-OAT) is useful for the identification of the relative contribution levels of influential factors to an objective system [27,28]. In this study, the LH-OAT method was implemented to quantitatively compare the effects of individual parameters on the backflow velocity of water from permeate to feed solutions in the membrane channel. The LH-OAT is a robust analysis method as compared to other global sensitivity analyses. One of its key advantages is relatively low computational load compared to other global sensitivity analyses such as one using Monte Carlo simulation because Latin Hypercube sampling allows controlling the total number of simulations [29]. Seven parameters were subject to sensitivity analysis and the ranges of their input values are summarized in Table 3. These are variables, controlled and designed by adjusting the operating conditions and selecting specific types of membranes in RO systems.

Table 3
Modeling parameters used in a sensitivity analysis.

Parameter (unit)	Min. value	Max. value
Water permeability, A (L m^{-2} h^{-1} bar^{-1})[a]	1.0	2.0
Solute permeability, B (L m^{-2} h^{-1})[a]	0.02	0.05
Membrane structure parameter, S (μm)[a]	685	1370
Average inlet velocity of solutions, $u_{1,\text{inlet}}$ and $u_{3,\text{inlet}}$ (cm/s)[b]	0.1	20
Inlet concentration of feed solution, $c_{1,\text{inlet}}$ (M)[c]	0.6	1.2
Inlet concentration of permeate solution, $c_{3,\text{inlet}}$ (M)[c]	0.002	0.04

[a] Parameters regarding intrinsic membrane properties were obtained based on commercially available RO membranes.

[b] Note that the sensitivity analysis involved crossflow velocity in the permeate channel, $u_{3,\text{inlet}}$, in an attempt to further investigate the relative importance of $u_{3,\text{inlet}}$ on OBW, despite the practical difficulty of velocity control in RO SWMs existing.

[c] Concentrations of feed and permeate solutions are in the ranges of 35,064–70,128 and 117–2338 mg/L, respectively.

$$S_{i,j} = \left| \frac{100 \times \left\{ \frac{M(e_1, \ldots, e_i(1+f_i), \ldots, e_p) - M(e_1, \ldots, e_i, \ldots, e_p)}{[M(e_1, \ldots, e_i(1+f), \ldots, e_p) + M(e_1, \ldots, e_i, \ldots, e_p)]/2} \right\}}{f_i} \right| \quad (5)$$

where $S_{i,j}$ is the partial sensitivity for a parameter e_i, M is the model function, f indicates the fraction by which the parameter e_i is changed, and j denotes an LH point.

3. Results and discussion

3.1. Influence of cross-flow velocity and spacer geometries on concentration profiles and backwash velocity

The spacer filament configurations can change hydrodynamic conditions in the flow channel, therefore resulting in different characteristics of the water and solute transport of membranes in SWMs [17,18,22]. Three spacer configurations (i.e., the zigzag, cavity, and submerged filament patterns) in the feed channels were selected and compared to an open channel (i.e., without spacers). In practical operation, the OBW can be implemented either by maintaining the feed flow at the feed-side applied pressure below the osmotic pressure difference between given solutions [6] or stopping these as quickly as possible to minimize the shift time between RO and OBW processes [8]. Hence, these two distinct conditions for OBW processes were considered in this study and referred to as Case 1 and Case 2: the former is operation with sufficient crossflow at an average inlet velocity of 10 cm/s, while the latter is that much lower crossflow at 0.1 cm/s. Note that TMP is absent from both cases.

Crossflow velocity is an operating parameter that influences CP. An increase in crossflow velocity can elevate shear stress on membrane surfaces, therefore enhancing mass transfer [25]. Without spacers (i.e., the open channels), Case 1 with the greater crossflow velocity resulted in a relatively uniform concentration profile throughout the feed channel and biofilm layer compared to Case 2 (Fig. 2), suggesting that the increased velocity enhanced the mass transfer in the vicinity of the membrane and fouling layer. With spacers, two distinct concentration profiles were observed between spacers that are adjacent to membrane surfaces (CS and ZS) and not adjacent (SS). The steeper concentration gradients were observed near the spacers adjacent to the membrane surfaces inside the biofilm layers in CS and ZS, whereas the spacers compressed a concentration boundary layer on the fouled membrane at the corresponding longitudinal coordination in SS. In the feed channel, the stagnant zone occurs near the spacer attachments to the membranes (Figs. S2 and S3). In RO membrane operations (not backwashing mode), spacers disrupt CP layers, and such disruption can effectively increase overall mass transfer efficiency, therefore increasing the permeate flux [30]. However, in osmotically driven membrane processes such as FO and PRO that have similar transport mechanisms with the OBW, the boundary layer disruption is still effective, but may not complement significant CP in the stagnant zones near the fouled membrane surfaces to which spacers are adjacent or attached [17]. In addition, the boundary layer disruption was found to be dependent on the crossflow velocity. Case 2 (i.e., lower velocity) showed the gradual development of concentration boundary layer along the flow direction (i.e., no boundary layer disruption), whereas Case 1 (i.e., higher velocity) showed a constant pattern of concentration profiles with respect to the spacer locations, evidence of boundary layer disruption.

Both crossflow velocity and spacer geometry also influenced the patterns of vortices and the location of stagnant zones (Figs. S1–S4). For the configurations in which spacers are adjacent to membrane surfaces, the higher velocity (Case 1) enlarged the areas of the vortices and stagnant zones behind the spacers on fouled membranes, while Case 2 (i.e., lower velocity) caused the vortices near the spacers with relatively small areas, thereby smaller area of stagnant zones (Fig. 2 and Figs. S2 and S3). The result suggests that such difference in hydrodynamic conditions, induced by distinct spacer geometries, can cause a spatially variable foulant removal efficiency along the feed channel during the OBW. This variability would be more significant for CS and ZS than SS. Besides, when comparing the absolute values of the wall shear stress on the fouled membrane surfaces, CS and ZS showed 0.70 (4.06×10^{-4}–1.22) and 1.56 (4.82×10^{-4}–8.92) on average, respectively, while SS exhibited 2.26 (0.57–9.25) (Case 1 in Fig. S5). This result also infers that both CS and ZS configurations might incur a reduced removal of biofilms near the spacers, owing to decreasing the crossflow-induced shear stress. As compared to CS, nevertheless, ZS had a higher mass transfer near the fouled membrane surfaces at which the upper spacers are embedded (such as at x/L of 0.25–0.40). The average wall shear stresses on the membrane surface at the corresponding longitudinal location were 3.34 and 0.57 for ZS and CS, respectively, and therefore ZS could possess the higher backwash velocity at the corresponding coordinates.

To scrutinize the water and salt mass transport in the open and spacer-filled channels for Case 1 and Case 2 shown in Fig. 2, we evaluated backwash velocity and biofilm-enhanced concentration polarization (newly termed 'dilutive BECP' in this study) for both cases (Fig. 3). The graphs in the top row demonstrate the benefit of the higher crossflow velocity on the backwash velocity for all the tested channel geometries. The backwash velocities in Case 1 increased slightly along the crossflow direction. It could be attributed to the salt mass transfer enhanced increasingly along the crossflow direction due to the greater osmotic backflow (therefore, the faster crossflow velocity along the channel). Those for Case 2, in contrast, abruptly dropped near the entrance of feed flow (at near $x = 0$ cm) and then gradually decreased. According to the graphs in the bottom row, the dilutive BECP profiles were also similar to the backwash velocity profiles, but BECP modulus declined along the dimensionless channel length for both Case 1 and Case 2, unlike the trends of backwash velocity. Nonetheless, a difference in dilutive BECP between inlet ($x/L = 0$) and outlet ($x/L = 1$) was much lesser for Case 1 than Case 2, which averaged ~13% and ~35%, respectively.

With spacers, much lower backwash velocities (therefore, lower dilutive BECP) were observed in the vicinity of the spacers adjacent to membrane surfaces for both Case 1 and Case 2. In addition to the extent, the backwash profiles were different depending on the spacer filament configurations. To be specific, the steep backwash velocity drops were observed at the longitudinal locations of spacers for CS and ZS, whereas a few increases in the backwash velocity were observed at the same longitudinal locations for SS. This indicates that the faster flows across the narrow gaps between filaments and membrane surfaces in SS yielded greater mass transfer rates than CS and ZS. Further, SS with the higher crossflow velocity would be more desirable to enhance the OBW efficiency in terms of biofilm removal, particularly in the

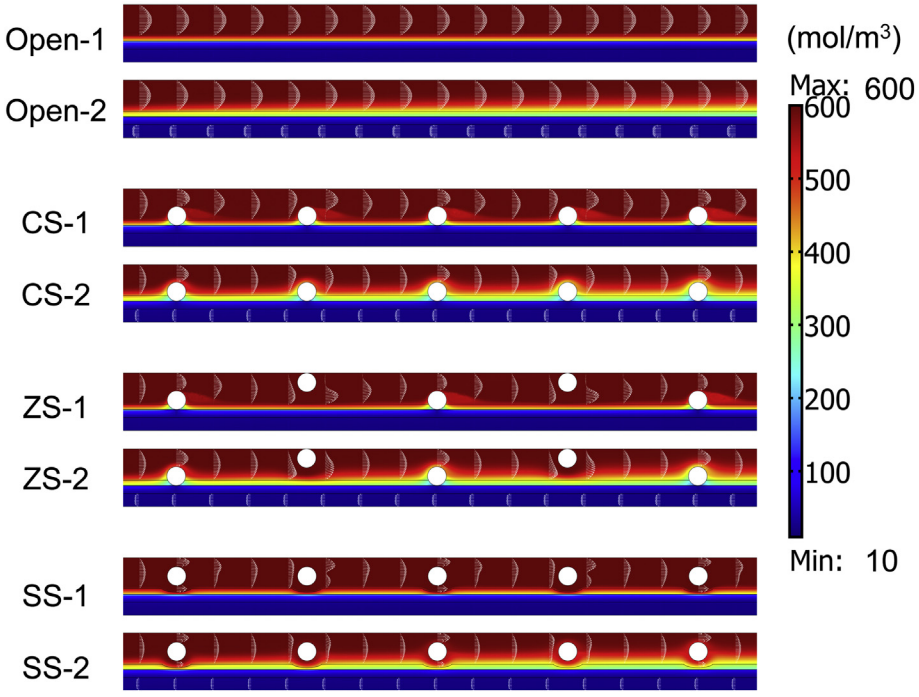

Fig. 2. Concentration contours of open channels and spacer-filled channels employing cavity, zigzag, submerged patterns of transverse filament configurations under two district operating conditions of osmotic backwash (OBW) process. The labels with 1 and 2 refer to Case 1 ($u_{1,inlet}$ = 10 cm/s) and Case 2 ($u_{1,inlet}$ = 0.1 cm/s), respectively.

vicinity of spacers. In RO operations, membrane surfaces are not evenly fouled and a greater extent of biofouling [31] and inorganic scaling [32] is often observed near spacer attachments. The backwash velocity of SS in Case 2 was average ~20% lower than that in Case 1 (Fig. 3c), which infers that such a low backwash velocity, incurred by insufficient crossflow like Case 2, may not be enough to remove biofilms near the spacer attachment.

3.2. Effect of fluid dynamics and membrane properties on concentration polarization

Section 3.1 suggested that crossflow velocity affected the extents of backwash flux and concentration profiles along the membrane channel. As shown in the top row of Fig. 4a, we observed a much thicker mass boundary layer in the feed channel at the lowest crossflow velocity (i.e., 0.1 cm/s). As increasing the crossflow velocity, the concentration profile change with respect to y/H became steeper, suggesting the thinner mass boundary layer (thereby, the lower dilutive ECP) and eventually the higher concentration inside a biofilm layer. For instance, a salt concentration at the membrane active layer surface, located at y/H = ~0.37 between biofilm and support layers, substantially rose from ~252 mol/m^3 to ~321 mol/m^3, as increasing the crossflow velocity from 0.1 cm/s to 1 cm/s. Interestingly, we found no noticeable differences in the mass boundary layer thickness when the velocity was 5 cm/s or above: the Sherwood number (Sh), defined as the ratio of the convective mass transfer to the diffusive mass transport, was 0.35, 0.41, 0.47, 0.49, and 0.52 at 0.1, 1, 5, 10, and 20 cm/s, respectively, exhibiting a slower growing rate of the convective mass transfer compared to the increment of crossflow velocity, particularly more significant at 5–20 cm/s than 0.1–5 cm/s. Also, the membranes with different transport properties showed a similar tendency of the concentration profile change depending on crossflow velocity (Fig. 4b and

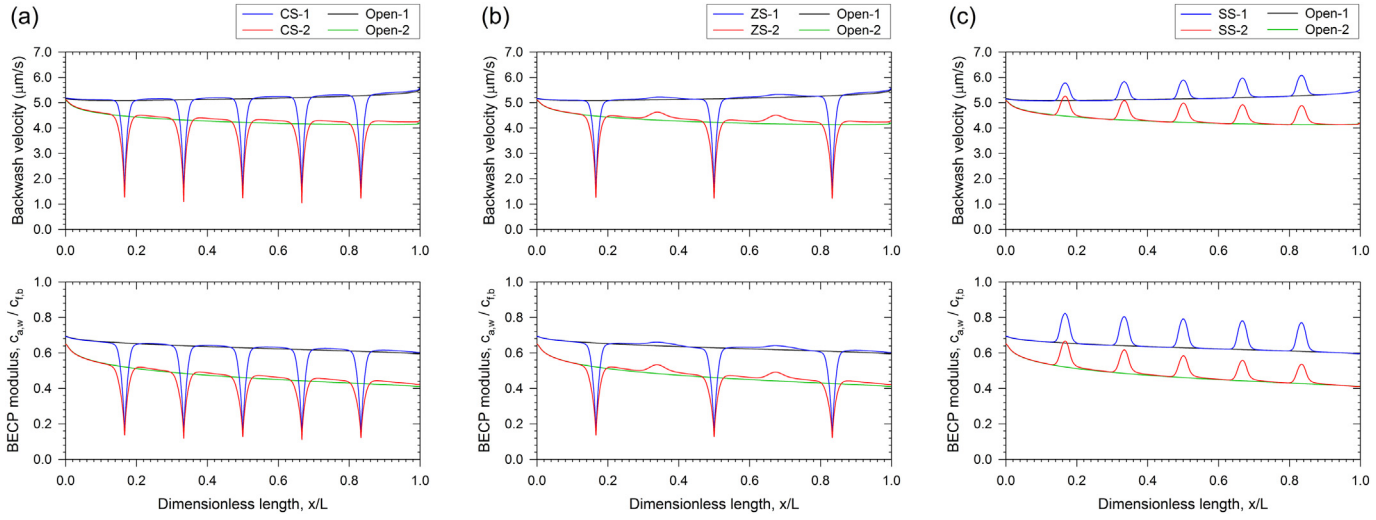

Fig. 3. Comparisons of backwash velocity and dilutive biofilm-enhanced concentration polarization (BECP) for channels with (a) cavity, (b) zigzag, and (c) submerged patterns of consecutive transverse filaments configurations compared to open channel. Note that the upper and lower color lines plotted in each graphs are obtained from two distinct simulations under Case 1 ($u_{1,inlet}$ = 10 cm/s) and Case 2 ($u_{1,inlet}$ = 0.1 cm/s), respectively.

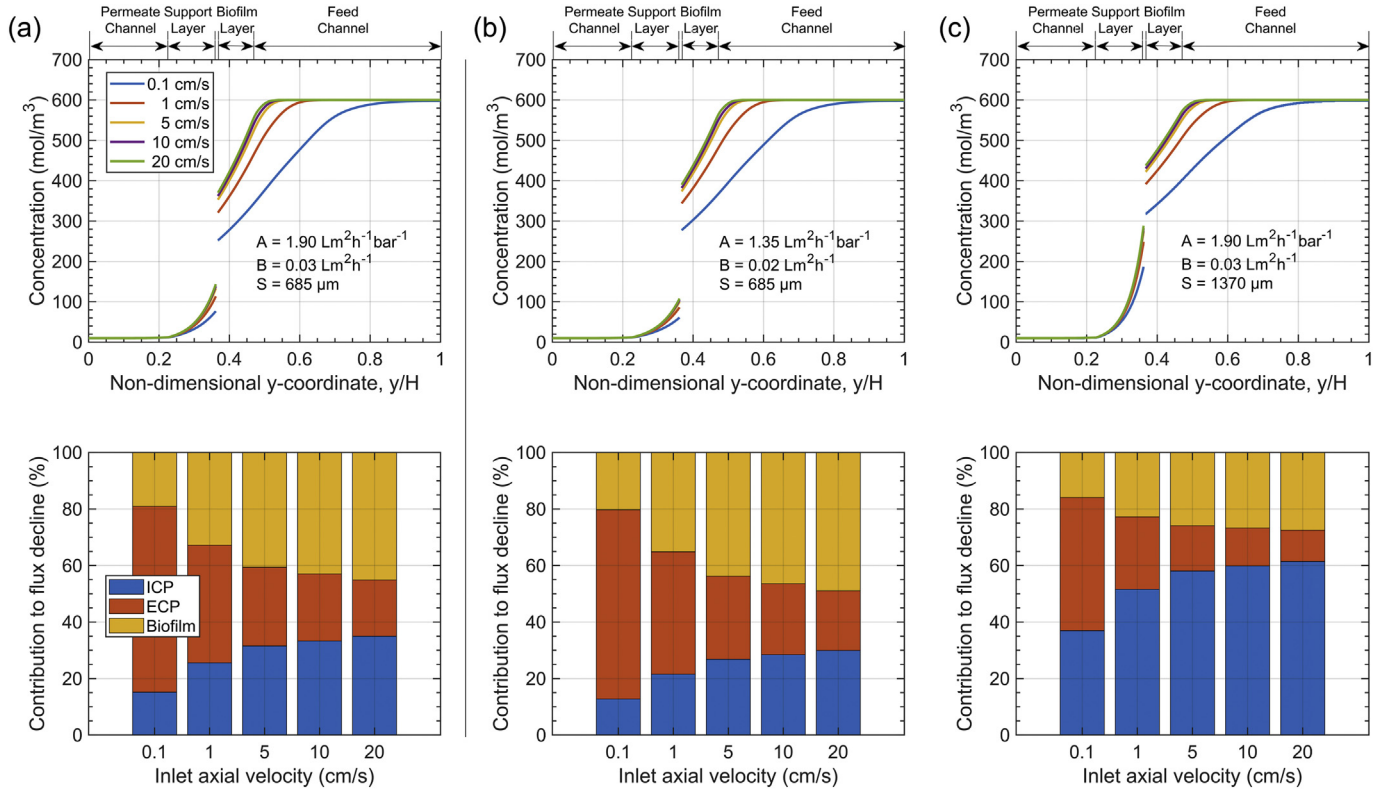

Fig. 4. Comparisons of OBW processes with RO membranes of (a) high permeability and low structure parameter, (b) low permeability and low structure parameter, and (c) high permeability and high structure parameter. In panels a–c, the upper row shows salt concentrations across the membrane, whereas the lower row shows the relative contributions of concentrative ICP and dilutive ECP, and dilutive BECP on backwash flux degradation under different crossflow velocities. Note that the parameters *A*, *B*, and *S* were selected to consider the high and low water permeability, solute selectivity, and physical stability within the acceptable range of those for commercially available thin-film composite (TFC) seawater RO membranes [33,34].

c), implying that an increased OBW efficiency due to an increase in crossflow velocity would not complement an increased energy consumption of a hydraulic pump. Although the overall trend concerning the crossflow velocity was similar, the extents of dilutive ECP, dilutive BECP, and concentrative ICP depended significantly on the membrane intrinsic properties such as water permeability (*A*), salt permeability (*B*), and membrane structure parameter (*S*).

The feed flow not only can directly disrupt the boundary layer in the vicinity of the fouled membrane surfaces (i.e., ECP) but also can indirectly influence mass transport inside the biofilm (i.e., BECP) as well as the membrane support layer (i.e., ICP). To understand the effects of each CP phenomenon on backwash velocity, their contributions to the flux decline were quantified and shown in the lower row of Fig. 4. The contribution has defined the ratio of backwash flux reduced by each CP to the ideal backwash flux without polarization. Remarkably, the inlet crossflow velocity in the feed channel had a substantial influence on the contribution of each CP to backwash velocity, even though it did not induce hydrodynamic mixing inside the biofilm and the support layer where BECP and ICP occur. At the lowest crossflow velocity (0.1 cm/s), the ECP showed the predominant effect on the backwash flux (~66% contribution), and its contribution to the backwash flux decline gradually reduced by ~20% as the inlet axial velocity increased to 20 cm/s (Fig. 4a). At 5 cm/s, BECP influenced the OBW dominantly at ~41%, followed by ICP and ECP at 32% and 28%, respectively. In addition, the membrane structure parameter (*S*) of the support layer impacted greatly on CP (Fig. 4a versus Fig. 4c). Doubling of membrane structure parameter, *S*, significantly increased the effects of ICP on the backwash flux (Fig. 4c versus Fig. 4a). This is in agreement with the previous numerical study of PRO membrane processes [25]. *S* is the effective path length that molecules travel through the membrane support layer. The higher *S* value means the longer path length through which molecules diffuse. Hence, *S* is the most important parameter determining ICP, which will be further explained later using the sensitivity analysis. In contrast, the membrane active layer properties including *A* and *B* marginally affected CP (Fig. 4a versus Fig. 4b).

3.3. Transmembrane pressure (TMP) and inlet feed and permeate concentrations

There is a threshold of the draw strength for effective foulant removal [5]. This infers that applying a high concentration of draw solution may be beneficial over TMP reduction that requires a long changeover time if the net driving force is sufficient to achieve a threshold of backwashing velocity. According to an operation manual for RO membrane elements [35], the feed flow and pressure are recommended to be increased or decreased by gradually adjusting the pump motor speed and the valve opening fraction, since sudden drastic changes in flow and pressure can permanently damage membranes, gauges, and valves of the system. In this sense, maintaining high TMP may be facile to switch between RO and OBW and minimize the changeover time. Besides, the benefits of lowering feed pressure would be marginal due to the high efficiency of the energy recovery device (ERD). Therefore, it would be beneficial to adjust the OBW solution concentration rather than changing TMP marginally.

The backwash velocity was evaluated under the following operating conditions in this study (Fig. 5): TMPs of 5, 10, and 20 bars; the inlet feed concentrations of 0.6 and 1.2 M (i.e., the typical ranges of seawater and concentrated RO brine, respectively); and the inlet permeate concentrations of 0.01 and 0.02 M (i.e., 500 and 1000 mg/L, respectively). When changing the inlet feed concentration from 0.6 to 1.2 M, the backwash velocity increased significantly to 44, 67, and 222% on average at a TMP of 5, 10, and 20 bars, respectively (Fig. 5a and b). In

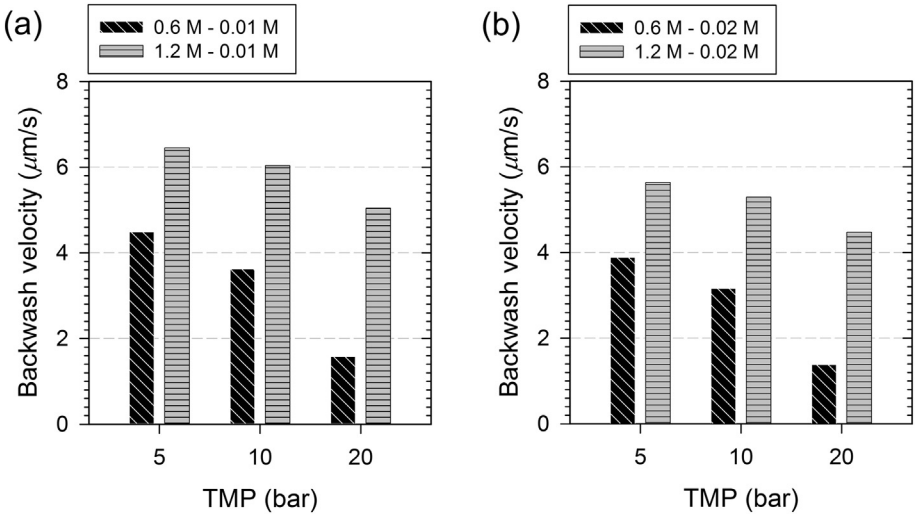

Fig. 5. Change in backwash velocity depending on a feed concentration and a transmembrane pressure (TMP) at (a) 0.01 M and (b) 0.02 M of permeate concentrations. Note that the backwash velocity is tested at an inlet velocity of 5 cm/s and 0.1 cm/s in feed and permeate channels, respectively.

addition, a 12.5% average reduction in the backwash velocity was observed as doubling the permeate concentration to 0.02 from 0.01 M (Fig. 5a versus b). Interestingly, the effects of feed concentration on backwash velocity change were more pronounced at the higher TMP. For 0.01 M of the permeate concentration (Fig. 5a), the difference of backwash velocity between 5 bar and 20 bar at the 1.2 M feed concentration was only ~22% while ~65% differential was observed for the 0.6 M feed concentration. A similar trend was observed for 0.02 M of the permeate concentration (Fig. 5b). This is because the net driving force (i.e., net osmotic pressure-TMP) at 20 bars of TMP was very low. The result implies that the application of a high concentration of draw solutions such as RO concentrate could be more beneficial to the cleaning efficiency [5].

Some existing experimental findings of the OBW qualitatively and quantitatively support the simulation results [5,12]. In Ramon et al.'s study [5], the cake-enhanced dilution effect, an analogous phenomenon of the dilutive BECP, due to a layer of alginate foulants diminished the backwash flow rate, which is in agreement with the simulation results of this study. Also, another study [12] showed a similar magnitude of backwash velocities (i.e., 3.6–6.9 μm/s) to the simulated values (i.e., 4.5–6.0 μm/s at 1.2 M and 10–20 bar) in the OBW for a biofouled RO membrane with a hypersaline flushing solution at 1.5 M and hydraulic pressure of 13.8 bar.

3.4. Sensitivity analysis of major factors

The previous sections demonstrated that many parameters could affect the OBW performance. Each parameter can influence one another; hence, it is challenging to delineate the impacts of each parameter on OBW efficiency. In order to comprehensively evaluate the effects of the individual parameter on OBW efficiency, a global sensitivity analysis using the LH-OAT method was implemented for seven important operational and design parameters such as A, B, S, average inlet crossflow velocities in the feed and permeate channels ($u_{1,\text{inlet}}$ and $u_{3,\text{inlet}}$, respectively), feed concentration (c_1) and permeate concentration (c_3).

Fig. 6 shows the results of the sensitivity analysis on the OBW process in the open and submerged spacer-filled channels in the presence and absence of a biofilm on a membrane surface. The sensitivity indices of each parameter were normalized by that of S, which has the highest value. It is noteworthy that the higher the sensitivity index is, the more influential for the backwash velocity. S was the most influential factor in all cases of the membrane channels, followed by c_1 and

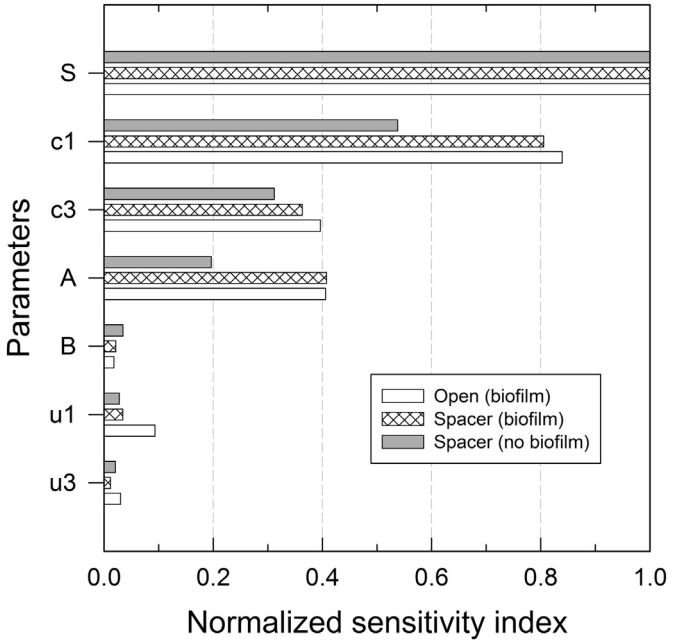

Fig. 6. Results of sensitivity analysis to rank influential parameters on the osmotic backwash (OBW) process for the open and spacer-filled channels in the existence and nonexistence of a biofilm. Note that a sensitivity value of each parameter is normalized by that of membrane structure parameter, S, that has the highest sensitivity.

c_3 for the spacer-filled channel without the biofilm, but c_1 and A for the open and spacer-filled membrane channels with the biofilm. The sensitivity index of A became doubled when membrane channels were biofouled for both the spacer-filled and spacer-free channels. Compared to S, nonetheless, intrinsic parameters of the membrane active layer, A and B, still exhibited much lower sensitivity index values. This result suggests that the selection of a membrane with a lower S would be the most effective means to enhance the OBW efficiency. To this end, a membrane with either thinner support layer, smaller tortuosity, or higher porosity can be selected to reduce the effective path length of diffusive salt flux, therefore reducing the extent of ICP. With a given membrane, the feed and permeate salt concentrations (c_1 and c_3, respectively) as well as the water permeability (A) are more influential than the salt permeability (B) and the crossflow velocities of the feed

and permeate streams (u_1 and u_3, respectively). Commercially available RO membranes, however, are generally required to possess a highly dense and compact structure of the thicker support layer for enduring a high-pressure ranging 40–70 bar for seawater desalination. With such a physical requirement of membrane property, optimizing A, c_1, and c_3 can be more practical to maximize the OBW efficiency. However, no noticeable difference in the sensitivity index between the spacer-filled channels with and without biofilm formation infers that spacer optimization may not be beneficial for the OBW efficiency practically.

4. Conclusion

Spacer and biofilm have considerable impacts on spatial changes in concentration and flow velocity of the membrane channel; therefore, the OBW efficiency. Considering the high complexity of the mass and momentum transport, incurred by the spacer and biofilm, accurate CFD simulation helps understand an OBW process in an SWM by describing reliable fluid dynamics in membrane channels with such complex geometry. In this study, we numerically modeled OBW processes using FEM to investigate the impact of intrinsic membrane properties and fluid dynamics on the OBW efficiency in the membrane channels with transverse spacer filaments and biofilm. The key conclusions of our model prediction results are summarized as follows:

- The submerged spacer, SS, showed higher shear stress and backwash flux at the longitudinal coordination of flow channels than the cavity and zigzag spacers, CS and ZS, respectively. The CS and ZS configurations, in which the spacers are adjacent to membrane surfaces, reduced the backwash velocity and incurred more dilutive BECP in the vicinity of the attachment regions of transverse filaments to the membrane. It implies that OBW with CS and ZS may not be sufficient to remove foulants, particularly in the spacer attachment regions, due to deteriorations in the crossflow-induced shear stress and the permeation drag of osmotic backflow of water.
- The fluid dynamics and the transport properties of membranes in the OBW process noticeably affect CP. Operation with low crossflow (≤ 1 cm/s) significantly aggravated the dilutive ECP, dilutive BECP, and concentrative ICP, whereas an increment in the crossflow velocity alleviated ECP and BECP, but there is little additional enhancement at > 5 cm/s. The effect of ECP on the backwash flux decline is more significant than those of BECP and ICP at the lower axial velocity in the inlet channel, but the latter two CPs increased gradually as raising the axial velocity and their contributions to backwash flux, in turn, become predominant at a high velocity (> 5 cm/s). Also, the membrane structure parameter, S, more significantly affected CP than the membrane active layer properties such as A and B.
- In a sensitivity analysis, the structure parameter of the porous support layer substantially impacted the OBW process of the RO membrane, while the water and salt permeabilities of the active layer play relatively marginal roles. Also, the existence of a biofilm in the flow channels can render c_1 and A more sensitive to the OBW process than the non-fouled channel.

Declaration of competing interest

The authors declare that they have no known competing financial interests or personal relationships that could have appeared to influence the work reported in this paper.

Acknowledgments

This research was supported by a research project tilted with 'Optimization of process and performance of SWRO modules applied with the osmotic backwash using the simulation and experimental approaches' funded by Hyundai Heavy Industries Co., Ltd.

Appendix A. Supplementary data

Supplementary data to this article can be found online at https://doi.org/10.1016/j.desal.2019.114229.

References

[1] L.F. Greenlee, D.F. Lawler, B.D. Freeman, B. Marrot, P. Moulin, Reverse osmosis desalination: water sources, technology, and today's challenges, Water Res. 43 (2009) 2317–2348.
[2] S.A. Snyder, S. Adham, A.M. Redding, F.S. Cannon, J. DeCarolis, J. Oppenheimer, E.C. Wert, Y. Yoon, Role of membranes and activated carbon in the removal of endocrine disruptors and pharmaceuticals, Desalination 202 (2007) 156–181.
[3] K. Jeong, M. Park, S.J. Ki, J.H. Kim, A systematic optimization of internally staged design (ISD) for a full-scale reverse osmosis process, J. Membr. Sci. 540 (2017) 285–296.
[4] V. Yangali-Quintanilla, Z. Li, R. Valladares, Q. Li, G. Amy, Indirect desalination of Red Sea water with forward osmosis and low pressure reverse osmosis for water reuse, Desalination 280 (2011) 160–166.
[5] G.Z. Ramon, T.-V. Nguyen, E.M. Hoek, Osmosis-assisted cleaning of organic-fouled seawater RO membranes, Chem. Eng. J. 218 (2013) 173–182.
[6] B. Liberman, I. Liberman, Replacing membrane CIP by direct osmosis cleaning, INTERNATIONAL DESALINATION AND WATER REUSE QUARTERLY 15 (2005) 28.
[7] J.P. Chen, S. Kim, Y. Ting, Optimization of membrane physical and chemical cleaning by a statistically designed approach, J. Membr. Sci. 219 (2003) 27–45.
[8] A. Sagiv, R. Semiat, Backwash of RO spiral wound membranes, Desalination 179 (2005) 1–9.
[9] G. Ramon, Y. Agnon, C. Dosoretz, Dynamics of an osmotic backwash cycle, J. Membr. Sci. 364 (2010) 157–166.
[10] J.-J. Qin, B. Liberman, K.A. Kekre, Direct osmosis for reverse osmosis fouling control: principles, applications and recent developments, The Open Chemical Engineering Journal 3 (2009) 8–16.
[11] J.-J. Qin, M.H. Oo, K.A. Kekre, B. Liberman, Development of novel backwash cleaning technique for reverse osmosis in reclamation of secondary effluent, J. Membr. Sci. 346 (2010) 8–14.
[12] E. Bar-Zeev, M. Elimelech, Reverse osmosis biofilm dispersal by osmotic backflushing: cleaning via substratum perforation, Environmental Science & Technology Letters 1 (2014) 162–166.
[13] J. Park, W. Jeong, J. Nam, J. Kim, J. Kim, K. Chon, E. Lee, H. Kim, A. Jang, An analysis of the effects of osmotic backwashing on the seawater reverse osmosis process, Environ. Technol. 35 (2014) 1455–1461.
[14] A. Sagiv, R. Semiat, Parameters affecting backwash variables of RO membranes, Desalination 261 (2010) 347–353.
[15] A. Sagiv, R. Semiat, Modeling of backwash cleaning methods for RO membranes, Desalination 261 (2010) 338–346.
[16] A. Sagiv, N. Avraham, C.G. Dosoretz, R. Semiat, Osmotic backwash mechanism of reverse osmosis membranes, J. Membr. Sci. 322 (2008) 225–233.
[17] M. Park, J.H. Kim, Numerical analysis of spacer impacts on forward osmosis membrane process using concentration polarization index, J. Membr. Sci. 427 (2013) 10–20.
[18] A. Subramani, S. Kim, E.M. Hoek, Pressure, flow, and concentration profiles in open and spacer-filled membrane channels, J. Membr. Sci. 277 (2006) 7–17.
[19] S. Ma, L. Song, Numerical study on permeate flux enhancement by spacers in a crossflow reverse osmosis channel, J. Membr. Sci. 284 (2006) 102–109.
[20] J. Schwinge, P. Neal, D. Wiley, D. Fletcher, A. Fane, Spiral wound modules and spacers: review and analysis, J. Membr. Sci. 242 (2004) 129–153.
[21] C. Koutsou, A. Karabelas, T. Goudoulas, Characteristics of permeate-side spacers of spiral wound membrane modules, Desalination 322 (2013) 131–136.
[22] A. Radu, J. Vrouwenvelder, M. Van Loosdrecht, C. Picioreanu, Modeling the effect of biofilm formation on reverse osmosis performance: flux, feed channel pressure drop and solute passage, J. Membr. Sci. 365 (2010) 1–15.
[23] S.S. Bucs, A.I. Radu, V. Lavric, J.S. Vrouwenvelder, C. Picioreanu, Effect of different commercial feed spacers on biofouling of reverse osmosis membrane systems: a numerical study, Desalination 343 (2014) 26–37.
[24] H. Brinkman, A calculation of the viscous force exerted by a flowing fluid on a dense swarm of particles, Flow, Turbulence and Combustion 1 (1949) 27.
[25] M. Park, J.J. Lee, S. Lee, J.H. Kim, Determination of a constant membrane structure parameter in forward osmosis processes, J. Membr. Sci. 375 (2011) 241–248.
[26] A.L. Zydney, Stagnant film model for concentration polarization in membrane systems, J. Membr. Sci. 130 (1997) 275–281.
[27] A. van Griensven, T. Meixner, S. Grunwald, T. Bishop, M. Diluzio, R. Srinivasan, A global sensitivity analysis tool for the parameters of multi-variable catchment models, J. Hydrol. 324 (2006) 10–23.
[28] M. Park, T. Anumol, S.A. Snyder, Modeling approaches to predict removal of trace organic compounds by ozone oxidation in potable reuse applications, Environmental Science: Water Research & Technology 1 (2015) 699–708.
[29] K. Holvoet, A. van Griensven, P. Seuntjens, P. Vanrolleghem, Sensitivity analysis for hydrology and pesticide supply towards the river in SWAT, Phys. Chem. Earth A/B/C 30 (2005) 518–526.
[30] V. Geraldes, V. Semião, M.N. de Pinho, The effect of the ladder-type spacers configuration in NF spiral-wound modules on the concentration boundary layers disruption, Desalination 146 (2002) 187–194.
[31] S.R. Suwarno, X. Chen, T.H. Chong, V.L. Puspitasari, D. McDougald, Y. Cohen, S.A. Rice, A.G. Fane, The impact of flux and spacers on biofilm development on

reverse osmosis membranes, J. Membr. Sci. 405–406 (2012) 219–232.
[32] T. Tran, B. Bolto, S. Gray, M. Hoang, E. Ostarcevic, An autopsy study of a fouled reverse osmosis membrane element used in a brackish water treatment plant, Water Res. 41 (2007) 3915–3923.
[33] S.S. Manickam, J. Gelb, J.R. McCutcheon, Pore structure characterization of asymmetric membranes: non-destructive characterization of porosity and tortuosity, J. Membr. Sci. 454 (2014) 549–554.
[34] A. Tiraferri, N.Y. Yip, A.P. Straub, S.R.-V. Castrillon, M. Elimelech, A method for the simultaneous determination of transport and structural parameters of forward osmosis membranes, J. Membr. Sci. 444 (2013) 523–538.
[35] Toray, Operation, Maintenance and handling manual for membrane elements, Available on, 2019. https://www.toraywater.com/knowledge/pdf/HandlingManual.pdf.